Investigation of Aerosol Formation During Benzaldehyde Photolysis

S. N. Dubtsov,* G. G. Dultseva, E. N. Dultsev, and G. I. Skubnevskaya

Institute of Chemical Kinetics and Combustion SB RAS, Institutskaya str., 3, Novosibirsk, 630090, Russia

Received: September 29, 2005; In Final Form: October 28, 2005

The kinetics of photolysis and photonucleation of benzaldehyde (BA) vapor in the air and in an inert gas is investigated, along with the physical and chemical characteristics of the resulting aerosol particles. Short-lived free radicals that accompany the BA photonucleation process were identified by means of spin trapping. Numerical simulation of BA photonucleation, combined with the proposed chemical mechanism, allowed us to calculate the rate of generation of initial particles and to estimate the aerosol quantum yield.

1. Introduction

Photochemically induced formation of nanosized aerosol particles may be the initial stage of the effective removal channels for some atmospheric pollutants including sulfur and nitrogen oxides, olefins, and aldehydes. The resulting particles can be scavenged by the surface of larger aerosol particles, and thus they make their contribution into the optical and radiative characteristics of the atmosphere.[1] Photochemically induced nucleation was observed both in the polluted urban atmosphere and in rural areas.[2] Despite the fact that the organic components of the submicrometer fraction of atmospheric aerosol account for about 10−60% of the total mass, the formation pathways for such compounds are poorly understood, in comparison with those for the sulfate and nitrate components. The reasons are due to both the complexity of the particles' chemical composition and the complexity of chemical reactions leading to aerosol formation. Although many laboratory studies of photochemically induced aerosol formation have been carried out,[3−6] many features of this process are still unclear and need further investigation. Therefore, the investigation of chemical mechanisms ending with the formation of organic nanoparticles and the estimation of aerosol yield during photochemical decomposition of individual compounds are important and timely problems in atmospheric chemistry.

Benzaldehyde (BA) is an important intermediate of photooxidation of some aromatic hydrocarbons, for example toluene. BA is always present in detectable amounts (along with formaldehyde and acetaldehyde) in the polluted urban atmosphere. For instance, undiluted emissions of engines may contain BA up to several hundred ppb. BA is photolyzed by the UV-wavelength part of sunlight with rather high efficiency.[7] Some products of BA photolysis can undergo gas-to-particle conversion. The photolysis of BA was investigated earlier,[8,9] but attention was mainly paid to the analysis of major gas products,[10] while the formation mechanism and composition of the condensed products were not as thoroughly investigated.

In the present paper, we describe the results of experimental investigation of the aerosol particle formation and growth during BA photolysis, determine chemical composition of the particles, and estimate the aerosol yield.

* Corresponding author.Telephone: +7-383-2-33-15-19. Fax: +7-383-2-34-23-50.

2. Experimental Section

2.1. Materials. BA ("chemically pure" grade) was twice distilled under reduced pressure before experiments. Just before the experimental run, it was distilled once more in argon flow at atmospheric pressure (T_{boil} = 176−177 °C). Compressed gases (O_2 "high pure" and N_2 "high pure") were used without additional purification, except for aerosol impurities; they were removed with HEPA filters. The BA concentration in the reagent mixture was determined with HP8354 spectrophotometer by measuring the absorption at λ = 233 nm in the flow cylindrical cell (l = 82 mm). For verification, the BA concentration was independently determined by bubbling the reagent flow with BA vapor through the solution of 2,4-dinitrophenylhydrazine. The resulting hydrazone concentration was measured with HPLC using "Milikhrom-1" chromatograph with microcolumns filled with the LiChrosorb sorbent.[11] An acetonitrile−water (3:1) mixture was used for elution. The concentration of the hydrazone formed was determined by measuring the UV absorption at λ = 360 nm.

Chemical analysis of the aerosol products was carried out using GC − MS (HP6890N/5973N). The aerosol particles were collected on glass fiber aerosol filters which were precleaned by heating above 400 °C in the air flow. The aerosol material was extracted with acetone ("high purity" grade) in an ultrasonic bath. NMR analysis of the aerosol products dissolved in CD_3CN was carried out with a Bruker DFX200 spectrometer. The ESR spectra of spin adducts were recorded with a Bruker ER-200 D-SRC spectrometer as described in detail elsewhere.[12]

Under static conditions, BA photolysis was carried out in a cylindrical cell (i.d. = 18 mm, l = 82 mm) with Suprasil windows; the irradiation source was the same as that in the aerosol experiments. A decrease in the concentration of BA was monitored with HP 8354 spectrophotometer by measuring the absorbance at 233 nm.

The aerosol formation kinetics was studied with the setup similar to that described elsewhere.[13,14] Figure 1 shows the schematic of the setup. It consists of the flow reactor (5) (22 mm inner diameter, ca. 300 mm length), low-pressure Hg lamp DRT-240 (6), and a Novosibirsk-type automated diffusion battery (NADB). The NADB consists of an eight-stage screen-type diffusion battery (7), a turbulent mixing condensation enlarger with dibutyl phthalate as a working liquid (8), photoelectrical particle counter (9), and microprocessor controller (10), which was used to run the NADB and to transfer the data to the PC (11).[14,15] The NADB allows measuring aerosol particle

10.1021/jp0555394 CCC: $33.50
Published on Web 12/08/2005

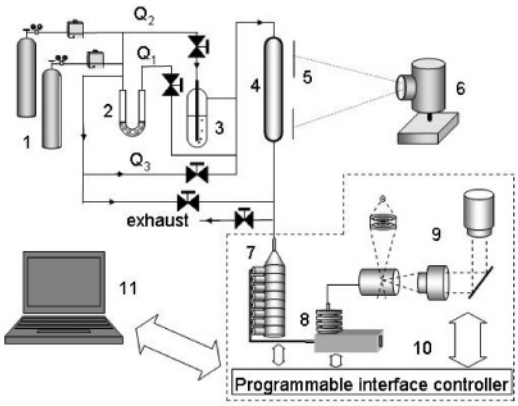

Figure 1. Schematic of the experimental set-up: (1) cylinders with compressed O_2 and N_2 with flow controllers; (2) U-shaped tube with BA; (3) bubbler with H_2O; (4) flow reactor; (5) slit; (6) UV-lamp; (7) diffusion battery; (8) condensation enlarger; (9) aerosol particle counter; (10) controller; (11) PC.

concentration from 10^1 to 10^7 cm^{-3} with ±10% accuracy[17] and size distribution from 2 to 200 nm, using a multiple solution averaging inversion procedure.[18] This inversion procedure was shown to reconstruct correctly multimodal size distributions and to resolve aerosol fraction with different size as separate peaks when the ratio of the mean diameters of fractions $R = D_a^{large}/D_a^{small}$ is larger than 2.5.[19] When the aerosol particle fractions have narrow size distribution (standard geometric deviation $\sigma_g = 1.1-1.2$), they can be resolved when R value is larger than 1.4.[20] The accuracies of determination of the mean arithmetic (D_a) and mean volume (D_v) diameters are ±7 and ±15% for D_a and D_v, respectively, as confirmed by comparing the results with those obtained using transition electron microscopy[21] and a TSI scanning mobility particle sizer model 3071.[20]

The flow of BA vapor (Q_1 = 0.1 L/min) is prepared by passing the carrier gas through the U-shaped tube filled with silica, impregnated with liquid BA (2). The tube is thermostated at 23 ± 1 °C. Then the gas flow with BA vapor is diluted with flows Q_2 and Q_3. The flow Q_2 passes through the bubbler with bidistilled water. The rates of these flows are varied from 0 to 0.1 L/min in such a way that the resulting flow ($Q_2 + Q_3$) is 0.1 L/min. This allows us to vary water concentration in the resulting reagent mixture from ca. 1.4×10^{15} to 2×10^{17} cm^{-3}. Water concentration is measured with Center 310 humidity meter with the ±2.5% accuracy. Then the final flow ($Q_1 + Q_2 + Q_2$) is passed through the reactor. The BA concentration in the reagent mixture is kept at 1.56×10^{16} cm^{-3} with an accuracy of ±5%. The aerosol particles are formed in the reactor under UV irradiation through the side wall. The irradiation time is varied from 1 to 30 s by changing the irradiated volume of the reactor with the slit (5). Immediately after having passed through the reactor, the flow containing the aerosol particles is diluted with the pure carrier gas to 1.1 L/min. The resulting flow is divided into two parts; the first one (1.0 L/min) goes to NADB, while another passes through the aerosol filter and then into the vent.

2.2. Benzaldehyde Photolysis Kinetics. We studied the dependence of the photolysis rate of BA vapor in nitrogen on the concentrations of water vapor and oxygen added into the gas mixture. The irradiation intensity was the same as in the aerosol experiments. A decrease in BA concentration follows the first order kinetics. The photolysis rate constant was found to be independent of the initial BA concentration and to be slightly dependent on oxygen concentration (Figure 2). D_0 and D represent BA absorbance at 233 nm before photolysis and during photolysis, respectively. Figure 3 shows that an increase

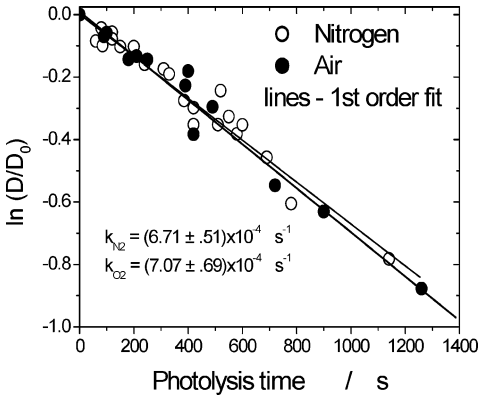

Figure 2. Photolysis kinetics of BA. [PhCHO] = 1.56×10^{16} cm^{-3}. Key (○) in pure N_2; (●) [O_2] = 6.64×1018 cm^{-3}; dots, experimental data; lines, least-squares linear fit.

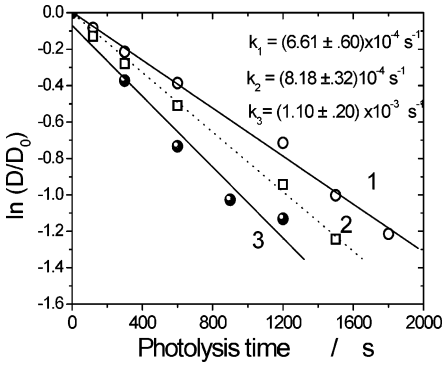

Figure 3. Influence of water on BA photolysis in N_2. [PhCHO] = 1.56×10^{16} cm^{-3}. Key: (1) [H_2O] = 1.41×10^{15} cm^{-3}; (2) [H_2O] = 8.78×10^{16} cm^{-3}; (3) [H_2O] = 2.06×10^{17} cm^{-3}.

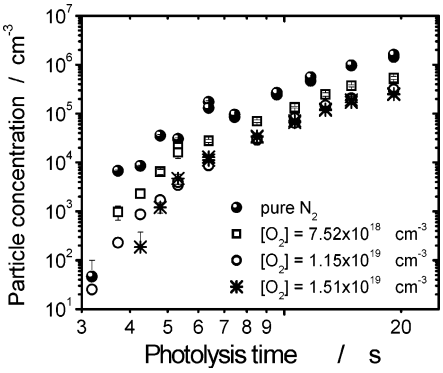

Figure 4. Influence of O_2 on the aerosol formation kinetics at PhCHO photolysis. [PhCHO] = 1.56×10^{16} cm^{-3}; [H_2O] = 1.41×10^{15} cm^{-3}.

in water concentration causes an increase in BA photolysis rate. This effect does not depend on the presence of O_2. The effective first-order rate constants were calculated using the slope of the kinetic curves; these rate constants were used to estimate the aerosol yield. If a Pyrex glass plate (2 mm thick, $\lambda_{cut-off}$ = 290 nm) is placed between the reactor and UV lamp, no decrease in BA concentration is observed during irradiation for 30 min. This means that the benzaldehyde photolysis in our experiments is induced by UV irradiation with the wavelength from 224 to 284 nm.

2.3. Aerosol Formation Kinetics of Benzaldehyde. The dependence of aerosol concentration on irradiation time (Figure 4) during BA photolysis is typical for the photochemically induced aerosol formation with a constant source of condensing products.[13] When the photolysis time (t_{phot}) increases from 3 to 6 s, the particle concentration (N_a) increases by a factor of 3000.

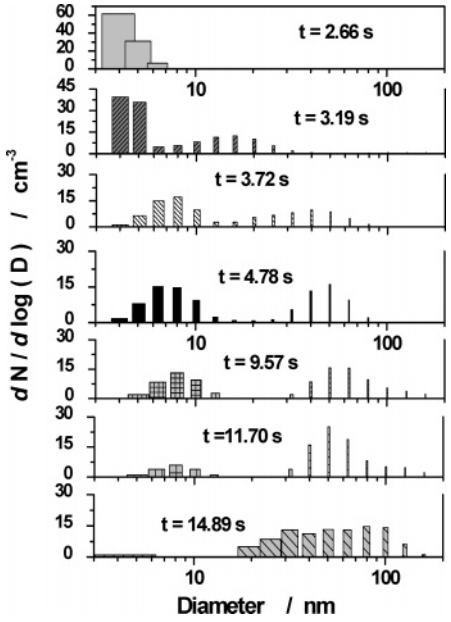

Figure 5. Example of the normalized particle size distribution time evolution. Benzaldehyde−N_2 photolysis. [PhCHO] = 1.56×10^{16} cm^{-3}; [H_2O] = 1.41×10^{15} cm^{-3}.

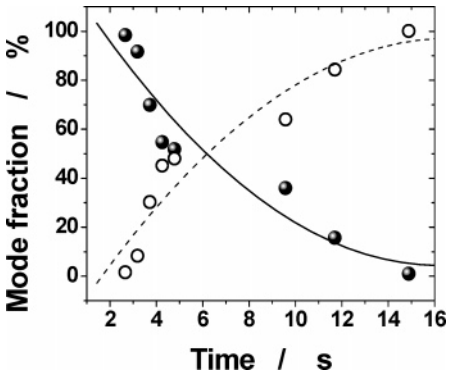

Figure 6. Change in the relative mode fraction. Key: small mode, from 2 to 15 nm in diameter; large mode, from 15 to 200 nm in diameter. [PhCHO] = 1.56×10^{16} cm^{-3}; [H_2O] = 1.41×10^{15} cm^{-3}.

At t_{phot} value greater than 10 s, the particle concentration is almost linear with time. It follows from Figure 4 that an increase in O_2 concentration in the reagent mixture leads to a decrease in the aerosol formation rate. The particles' mean arithmetic diameter increases with BA vapor irradiation time. The evolution of the particle size distribution with time is presented in Figure 5. The particle size distribution has two modes, the small one with a mean diameter of 5−8 nm and the large one with a mean diameter of 50−80 nm; there are no particles with intermediate size. The shape of the particle size distribution does not depend on [O_2]. These kinds of size distributions are typical for the coagulation growth of the particles in the presence of evaporation. A similar type of size distribution has been experimentally observed earlier for the photochemical aerosol formation of various organics.[20,22] Similar bimodal distributions were obtained in the numerical modeling of photochemically induced aerosol formation.[23] An increase in the mean particle diameter with irradiation time results from a decrease in the fraction of the small mode (Figure 6), while the modal diameter is almost constant with t_{phot} when t_{phot} is larger than 3.5 s. The aerosol mass, calculated from the aerosol particle volume assuming that the density of particle material is 1 g/cm^3, increases linearly with an increase in irradiation time. An increase in oxygen concentration in the reagent mixture results in a decrease in the aerosol mass generation rate (Figure 7).

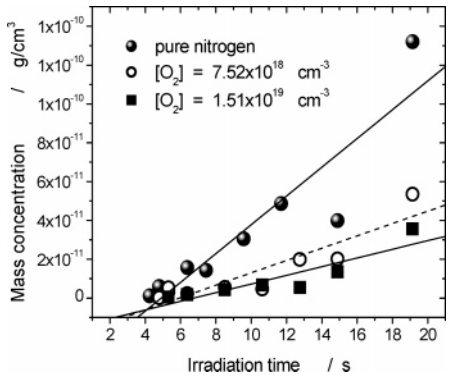

Figure 7. Influence of O_2 on the aerosol mass generation rate. [PhCHO] = 1.56×10^{16} cm^{-3}; [H_2O] = 1.41×10^{15} cm^{-3}. Key: (●) [O_2] = 0; (○) [O_2] = 7.52×10^{18} cm^{-3}; (■) [O_2] = 1.51×10^{19} cm^{-3}.

The influence of water on the aerosol formation kinetics during BA photolysis in nitrogen was also studied. Despite the fact that an increase in [H_2O] leads to an increase in the photolysis rate, the aerosol formation rate decreases with an increase in water concentration. The aerosol particle mass concentration is also linear with time and aerosol mass generation rate decreases with an increase in [H_2O].

3. Discussion

3.1. Aerosol Formation Yield. The aerosol formation yield φ_{aer} was calculated as a ratio of the aerosol mass formation rate W_{aer} to the BA photolysis rate W_{phot}:

$$\varphi_{aer} = W_{aer}/W_{phot} = (d(1/6\pi N d_v^3 \rho)/dt)/k_{phot}[PhCHO]$$

where N is particle number concentration (cm^{-3}), d_v is the mean volume particle diameter, k_{phot} is the rate constant of BA photolysis rate. The BA photolyzed mass was calculated from the photolysis kinetics, and the aerosol particle mass was calculated by integrating the particle size distribution, with the assumption that the particles' specific density is 1 g/cm^3. The aerosol yield was calculated from the experimental data shown in Figures 2−5 for different conditions; the yield is presented in Table 1. It follows from Table 1 that φ_{aer} value decreases with an increase in oxygen and water concentration. A rough estimate of aerosol yield during BA photolysis, made by Seinfeld and Pandis,[3] is 5 μg/m^3 ppm^{-1}, or about 1 mg/cm^3 per 1 g of the photolyzed BA, which makes 10^{-3}, which is very close to that obtained in this study. A decrease in the yield accompanying an increase in oxygen concentration can be qualitatively explained by an increase in the importance of photooxidation reactions. The aerosol accounts for only a minor part of the photooxidation products; the major products are gaseous. The chemical composition of aerosol and gas products also changes with an increase in O_2 concentration in the reaction mixture. A decrease in φ_{aer} value with an increase in water concentration is opposite to that observed for the photochemical aerosol formation in acetaldehyde vapor.[14] This can be explained by the fact that aerosol particles formed from acetaldehyde photolysis exhibit hydrophilic properties, while those formed from BA photolysis are hydrophobic.

3.2. Analysis of the Chemical Composition of the Gas and Aerosol Products of Benzaldehyde Photolysis. *3.2.1. Analysis of the Gas Products.* Gas products were analyzed using HPLC. Carbonyl compounds were analyzed in the form of hydrazones, resulting from the reaction of carbonyls with 2,4-dinitrophen-

TABLE 1: Benzaldehyde Photolysis Rates, Aerosol Formation Rates, and Aerosol Yield for Various Experimental Conditions

$[N_2]$, cm^{-3}	$[O_2]$, cm^{-3}	$[H_2O]$, cm^{-3}	W_{phot}, g/(cm^3 s)	W_{aer}, g/(cm^3 s)	φ_{aer}
2.69×10^{19}	0	$<2.36 \times 10^{15}$	1.81×10^{-9}	2.28×10^{-12}	1.26×10^{-3}
2.69×10^{19}	0	1.48×10^{17}	2.25×10^{-9}	1.98×10^{-12}	0.88×10^{-3}
2.69×10^{19}	0	2.06×10^{17}	3.02×10^{-9}	1.63×10^{-12}	0.54×10^{-3}
1.94×10^{19}	0.752×10^{19}	$<2.36 \times 10^{15}$	1.89×10^{-9}	1.01×10^{-12}	0.58×10^{-3}
1.53×10^{19}	1.15×10^{19}	$<2.36 \times 10^{15}$	1.70×10^{-9}	0.97×10^{-12}	0.57×10^{-3}
1.18×10^{19}	1.51×10^{19}	$<2.36 \times 10^{15}$	2.11×10^{-9}	0.73×10^{-12}	0.35×10^{-3}

TABLE 2: ESR Hyperfine Splitting Constants (a_N and a_H, mT) and Lifetimes (τ, min) of Spin Adducts Detected under BA Photolysis in Nitrogen and in Air with the HDPDO and PMIO Spin Traps

	in nitrogen			in air		
spin trap	a_N	a_H	τ	a_N	a_H	τ
HDPDO	1.68	2.57	24 (**1**)	1.47	1.51	48 (**4**)
	1.65	2.08	35 (**2**)			
	1.65		31 (**3**)			
PMIO	1.46	1.32	12 (**5**)	1.37	1.49	18 (**8**)
	1.41	1.84	31 (**6**)	9.2		22 (**9**)
	1.38		55 (**7**)			

TABLE 3: Physicochemical Characteristics of Aerosol Products, Formed During BA Photolysis in Air (AA) and in Nitrogen (AN)

characteristics	AN	AA
state, color	solid, light- gray	solid, white
melting temp, °C	78−84	78−81
solubility:	C_6H_6, $CHCl_3$	$CHCl_3$, CH_3CN
no. of components, HPLC (306−328 nm)	3	2

ylhydrazine. For BA photolysis in air, the only detected carbonyl product was BA itself. For the photolysis in N_2, benzophenone (ca. 0.3% of the photolyzed BA) and formaldehyde HCHO (ca. 0.6%) were found among the gaseous products of photolysis. The initial BA did not contain HCHO (the detection limit of the method used was 2 ng/m^3). The possible mechanism of HCHO formation in this case is the detachment of H$^\bullet$ atom by HCO$^\bullet$ radical from the BA aldehyde group. This process leads directly to the formation of phenoxyl radical PhCO$^\bullet$ and further to aerosol products. If the transformation really takes place in such a way, it becomes clear why the aerosol formation efficiency for BA photolysis in air is not so much different from that in inert gas as it was observed for acetaldehyde and formaldehyde photolysis[14,24] The most active radicals produced during photolysis in air and in nitrogen in the latter two systems sharply differ from each other in reactivity.

To identify short-lived free radicals accompanying BA photolysis, we used acyclic α-phenyl nitrone (PN), 1,2,2,5,5-pentamethyl-3-imidazoline-3-oxide (PMIO), and 3-hydroxy-2,3-dihydro-2,2,5-trimethylpyrazine-1,4-dioxide (HDPDO). The PN trap was used to establish the presence of short-lived free radicals in the mixture under photolysis. Both for mixtures with air and with nitrogen under irradiation with $\lambda < 290$ nm, we observed an ESR spectrum of PN spin adducts with hyperfine splitting constants (hsc) $a_N = 1.48$ mT, $a_H = 0.2$ mT. Small a_H values did not allow unambiguous identification of differences and reliable identification of the trapped radicals. Because of this, to identify the radicals, we used the PMIO and HDPDO traps, which are cyclic and thus give larger hsc constants (a_H).

With these cyclic spin traps, the formation of short-lived free radicals under benzaldehyde photolysis was also observed only under irradiation with the short-wavelength light (<290 nm). Different free radicals are formed under photolysis in air and in nitrogen. The results are listed in Table 2. The spin adducts of both HDPDO and PMIO formed under photolysis in nitrogen give a superposition of three ESR signals: two of them are triplets of doublets, and the third one is a triplet. In air, only one weak signal with $a_N = 1.47$ *mT*, $a_H = 1.51$ *mT* (**4**) is observed with HDPDO. With PMIO, a stronger ESR signal with $a_N = 1.37$ mT, $a_H = 1.49$ mT (**8**) is observed, along with a triplet (**9**).

On the basis of ESR hyperfine splitting constants of adducts, we assumed that **1** and **5** are the adducts with phenyl radical, while **2** and **6** are the adducts with formyl HCO. These radicals are known to be formed in the primary step of benzaldehyde photolysis under the UV light with wavelengths shorter than 280 nm:[7,8]

$$C_6H_5CHO + h\nu \rightarrow C_6H_5 + HCO$$

To confirm the kinds of radicals trapped, we generated HCO and phenyl photolytically using other initial compounds (formaldehyde; chlorobenzene) and detected the spin adducts with hyperfine splitting constants equal to those observed in the photolysis of BA.

The adducts formed in BA photolysis in air are characterized by a_H value typical for oxy radicals RO.[25,26] So, in the presence of oxygen we observe transformation of the primary radicals formed directly in benzaldehyde photolysis.

3.2.2. Analysis of Aerosol Products. Aerosol products of BA photochemical aerosol formation in air (AA) and in nitrogen (AN) are amorphous, slightly colored solids, with the melting temperature about 80 °C. They are well soluble in acetonitrile and partially soluble in benzene. Both AA and AN do not dissolve in diluted acids (H_2SO_4 and HCl). Some of their physicochemical properties are listed in Table 3.

Analysis by means of HPLC after the reaction with 2,4-dinitrophenylhydrazine showed that none of the AA and AN samples contained carbonyl groups. The IR absorption spectrum of the aerosol product formed under photolysis in nitrogen contains characteristic bands related to BA. This allows us to assume that the aerosol product contains fragments of photopolymer $(C_6H_5CHO)_n$, which is known to be formed under photolysis at 366 nm with quantum yield of about 0.1.[9] The IR spectrum of the aerosol product formed under photolysis in air contains bands related to BA, too, but they are much weaker than those observed for the AN product. In air, the predominant fraction is sharply different in solubility from the initial BA; it does not contain the phenyl fragment. This may be the product of oxidative opening of the ring. These results are confirmed by the data of ^{1}H NMR spectroscopy and GC-MS analysis. The most intensive lines in the NMR spectrum of the aerosol formed in nitrogen are typical for the compounds containing several benzene rings connected with each other through alkoxy groups, and the signal of OH group bound to the aromatic ring. In the NMR spectrum of the aerosol formed in the presence of oxygen, any lines related to the protons of the aromatic ring are almost absent.

On the basis of literature data and on the experimental results obtained in this study, the possible chemical mechanism of aerosol formation during BA photolysis in nitrogen and in air is proposed in Figures 8 and 9.

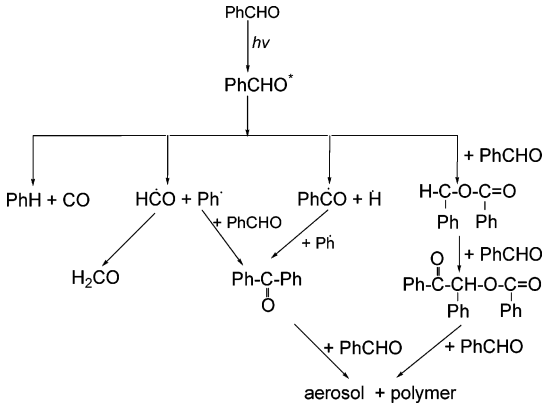

Figure 8. Proposed mechanism of aerosol products formation during benzaldehyde photolysis in N_2.

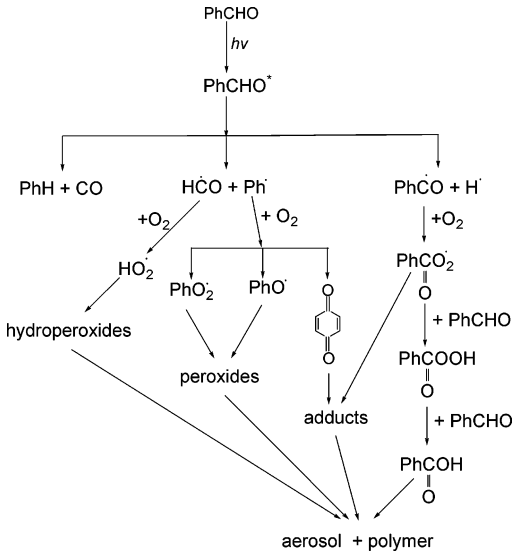

Figure 9. Proposed mechanism of aerosol products formation during benzaldehyde photolysis in air.

Here PhCHO* denotes either S^1 or T^1 excited states of BA. Because of the fast singlet − triplet conversion, it is not quite clear what states give rise to specific pathways. Nevertheless, comparison between reaction products and intermediates formed in inert gas and in the presence of oxygen suggests that the interaction of primary radicals with oxygen causes substantial changes in reaction pathways; oxygenated short-lived intermediates lead to essentially different products, both in the gas phase and in aerosol. As we have already mentioned, aerosol formed in nitrogen is composed mainly of BA oligomeric fragments, while that formed in air comprises quinone fragments and also the product of oxidative opening of the aromatic ring. So, the approach based on detailed physicochemical investigation of the intermediates and products of benzaldehyde photolysis allowed us to follow the mechanism of photochemical aerosol formation in benzaldehyde vapor.

4. Conclusions

Investigation of the kinetics of photochemical aerosol formation in BA showed that the yield of aerosol products is within the range 10^{-3} to 3×10^{-4} (when BA concentration is 1.56×10^{16} cm^{-3}**)**, depending on the composition of gas medium (carrier gas). An increase in water vapor content causes an insignificant increase in photolysis rate and a decrease in the aerosol formation rate. An increase in oxygen content of the reaction mixture causes a decrease in the aerosol formation rate and correspondingly a decrease in the yield of aerosol products.

Chemical composition of aerosol products changes with addition of oxygen into the reaction mixture. The data on chemical composition of gas and aerosol products of BA photolysis allow us to assume that the formation of nuclei of the dispersed phase occurs during gas-phase transformations of BA according to two types of mechanisms: photochemical polymerization and opening of the ring. In inert gas, phenyl radical formed in the primary photochemical step acts as an initiator of polymerization. The aerosol product is a mixture of fractions with different molecular masses, conserving the phenyl fragment in the structure of oligomeric molecules. In air, a product of oxidative opening of the ring is observed in the aerosol products in addition to the fraction containing the phenyl fragment; this allows us to conjecture that the process follows these two mechanisms; the preference between the two routes depends on the presence of oxygen.

Acknowledgment. The authors thank Dr. A. I. Kruppa for recording the NMR spectra of aerosol products, Dr. L. V. Kuibida for carrying out gas chromatographic−mass spectrometric examination. Financial support from CRDF, Project No. RC1-2330-NO-02, is gratefully acknowledged.

References and Notes

(1) *The chemistry of the atmosphere: its impact on global change: a chemistry for the 21st century monograph*; Calvert, Jack G., Ed.; Blackwell Science: New York, 1994; p 394.

(2) Kulmala, M.; Vehkamäki, H.; Petäjä, T.; Dal Maso, M.; Lauri, A.; Kerminen, V.-M.; Birmili, W.; McMurry, P. H. *J. Aerosol Sci.* **2004**, *35*, 143−176.

(3) Seinfeld, J. H.; Pandis, S. N. *Atmospheric Chemistry and Physics: From Air Pollution to Climate Change*; John Wiley: New York, 1997.

(4) Finlayson-Pitts, B. J.; Pitts, J. N. *Atmospheric Chemistry: Fundamentals and Experimental Techniques*; John Wiley: New York, 1986.

(5) Isidorov, V. A. *Organic Chemistry of the Atmosphere*; Khimizdat: St. Petersburg, 2001.

(6) Kleindienst, T. E.; Smith, D. F.; Li, W.; Edney, E. O.; Driscoll, D. J.; Speer, R. E.; Weathers, W. S. *Atmos. Environ.* **1999**, *33*, 3669−3681.

(7) Zhu, Lei; Cronin, T. J. *Chem. Phys. Lett.* **2000**, *317*, 227−231.

(8) Berger, M.; Goldblatt, I. L.; Steel, C. *J. Am. Chem. Soc.* **1973**, *95*, 1717−1725.

(9) De Mare, G. R.; Fox, J. R. *J. Photochem.* **1986**, *32*, 293−301.

(10) Almasy, F. *J. Chem. Phys.*. **1933**, *30*, 528, 634, 713.

(11) Skubnevskaya, G. I.; Dultseva, G. G. *J. Ecological Chem.* **1994**, *3*, 29−34.

(12) Dultseva, G. G.; Skubnevskaya, G. I.; Volodarsky, L. V.; Tikhonov, A. Ya.; Mazhukin, D. G. *J. Phys. Chem.* **1996**, *100*, 17523−17527.

(13) Dubtsov, S. N.; Levykin, A. I.; Sabelfeld, K. K. *J. Aerosol Sci.* **2000**, *31*, 509−518.

(14) Skubnevskaya, G. I.; Dubtsov, S. N.; Dultsev, E. N.; Dultseva, G. G.; Tsang, W. *J. Phys. Chem. B* **2004**, *108*, 11395−11398.

(15) Reischl, G. P.; Ankilov, A. I.; Baklanov, A. M.; Marliev, R. A.; Eremenko, S. I.; Majerowicz. *J. Aerosol Sci.***1991**, *12*, S325−S326.

(16) Reference deleted in proof.

(17) Ankilov, A.; Baklanov, A.; Colhoun, M.; Enderle, K. H.; Gras, J.; Julanov, Y.; Kaller, D.; Lindner, A.; Lushnikov, A. A.; Mavliev, R.; McGovern, F.; Mirme, A.; O'Connor, T. C.; Podzimek, J.; Preining, O.; Reischl, G. P.; Rudolf, R.; Sem, G. J.; Szymanski, W.W.; Tamm, E.; Vrtala, A. E.; Wagner, P. E.; Winklmayr, W.; Zagainov, V. *Atm. Res.* **2002,** *62*, 171−208.

(18) Eremenko, S. E.; Ankilov A. N. *J. Aerosol Sci.* **1995**, *26*, S749−S750.

(19) Eremenko, S. E.; Caldow, R.; Baklanov, A. M.; Havlicek, M.; Sem, G. *J. Aerosol Sci.* **1995**, *26*, S747−S748.

(20) Baklanov, A. M.; Dubtsov, S. N.; Caldow, R.; Havlicek, M.; Sem, G. *Aerosol Sci.* **1995**, *26*, S751−S752.

(21) Onischuk, A. A.; di Stasio, S.; Karasev, V. V.; Baklanov, A. M.; Makhov, G. A. Vlasenko, A. L.; Sadykova, A. R.; Shipovalov, A. V.; Panfilov, V. N. *Aerosol Sci.* **2003**, *34*, 383−403.

(22) Carlsson, R. S.; Szente, J. J.; Ball, J. C.; Maricq, M. M. *J. Phys. Chem. A* **2001**, *105*, 83−89.

(23) Rao, N. P.; McMurry, P. H. *Aerosol Sci. Technol.* **1992**, *11*, 120−132.

(24) Skubnevskaya, G. I.; Dubtsov, S. N.; Dultsev, E. N. *Atmos. Oceanic Opt.* **1997**, 429−432.

(25) Pryor, W. A.; Tamura, M.; Church D. F. *J. Am. Chem. Soc.* **1984**, *106*, 5073−5079.

(26) Migita, C. T.; Chaki, S.; Ogura, K. *J. Phys. Chem.* **1989**, *93*, 6368−6373.